Charge-mediated voltage modulation of magnetism in $Hf_{0.5}Zr_{0.5}O_2$/Co multiferroic heterojunction

Jia Chen(陈佳)[1,2], Peiyue Yu(于沛玥)[1,2], Lei Zhao(赵磊)[1,2], Yanru Li(李彦如)[1,2], Meiyin Yang(杨美音)[1], Jing Xu(许静)[1,2], Jianfeng Gao(高建峰)[1], Weibing Liu(刘卫兵)[1], Junfeng Li(李俊峰)[1], Wenwu Wang(王文武)[1,2], Jin Kang(康劲)[3], Weihai Bu(卜伟海)[3], Kai Zheng(郑凯)[3], Bingjun Yang(杨秉君)[4], Lei Yue(岳磊)[4], Chao Zuo(左超)[4], Yan Cui(崔岩)[1,‡], and Jun Luo(罗军)[1,2,†]

[1] *Institute of Microelectronics, Chinese Academy of Sciences, Beijing* 100029, *China*
[2] *University of Chinese of Academy Sciences (UCAS), Beijing* 100049, *China*
[3] *Semiconductor Technology Innovation Center (Beijing) Corporation, Beijing* 100176, *China*
[4] *ULVAC Research Center Suzhou CO., Ltd., Suzhou* 215026, *China*

(Received 20 August 2022; revised manuscript received 9 October 2022; accepted manuscript online 14 October 2022)

We construct the Hall-bar device with the size of several hundred nanometers based on the HZO/Co multiferroic heterojunction. A remarkable voltage-controlled magnetism is observed in the device that possesses both ferroelectric property and perpendicular magnetic anisotropy (PMA). The nucleation field and coercivity can be modulated by voltage pulse while saturation field keeps stable. The non-volatile and reversible voltage-controlled magnetism is ascribable to interfacial charges caused by ferroelectric polarization. Meanwhile, the effective anisotropy energy density (K_u) can also be controlled by voltage pulse, a decrease of 83% and increase of 28% in K_u are realized under −3-V and 3-V pulses, respectively. Because the energy barrier is directly proportional to K_u under a given volume, a decreased or enhanced energy barrier can be controlled by voltage pulse. Thus, it is an effective method to realize low-power and high-stability magneto-resistive random-access memory (MRAM).

Keywords: multiferroic heterojunction, voltage-controlled magnetism, energy barrier

PACS: 75.85.+t, 75.70.Cn, 77.55.Nv **DOI:** 10.1088/1674-1056/ac9a3b

1. Introduction

Nowadays, 22-nm/28-nm embedded magneto-resistive random-access memory (eMRAM) is already used in industrial production. For the continuous scaling down, the better performance such as low power consumption and high thermal stability are desired. The energy barrier which separates two stable magnetizations is a crucial factor that decides the power consumption of data writing and thermal stability for MRAM. During the data writing, a lower energy barrier favors lower power consumption. On the other hand, a higher energy barrier means better stability against thermal disturbance, which is beneficial to data retention.

Voltage-controlled magnetism is an effective method that can modulate magnetic behaviors such as coercivity, magnetization, magnetization switching, *etc*.[1–4] And it is also a useful way to control the energy barrier of magnetic material. The common forms of the voltage-controlled magnetism include voltage-controlled magnetic anisotropy (VCMA), magneto-ionic effect, and multiferroic structure, *etc*. VCMA is commonly adopted in ferromagnetic/dielectric material system, the accumulation or dissipation of electrons at the interface under different voltages can control magnetic anisotropy and change energy barrier.[5–7] While VCMA effect is volatile, it is hard to modulate thermal stability for a long time. Magneto-ionic effect is a method based on ion migration driven by electric field. Though magneto-ionic effect can impact magnetic property remarkably, it often needs long time, higher voltage or thermal assistance, which is not suitable for MRAM.[8–11] Ferroelectric/ferromagnetic composition is one of most studied multiferroic structures. Similarly, accumulation or dissipation of electrons at the interface can be realized due to ferroelectric polarization under different voltages. Unlike VCMA, the state of interfacial electrons can keep stable after the disappearance of voltage, which can achieve the target of lower energy barrier in data writing and higher energy barrier in data retention simultaneously.[12,13]

In this work, a multiferroic heterojunction comprised of HfO_2-based ferroelectric and Co ferromagnetic film is formed. Because of the reasonable design of film stacks and process, the heterojunction possesses both ferroelectricity and perpendicular magnetic anisotropy (PMA). The controllable magnetic behaviors including nucleation field, coercivity by different voltage pulses are found in Hall-bar device with the size of several hundred nanometers. Besides, through the cal-

†Corresponding author. E-mail: luojun@ime.ac.cn
‡Corresponding author. E-mail: cuiyan@ime.ac.cn

© 2023 Chinese Physical Society and IOP Publishing Ltd

culation of effective anisotropy energy density under different voltage pulses, an efficient modulation on energy barrier is observed. What is more, all the above voltage-controlled properties are reversible and non-volatile. Considering the ferroelectricity, we attribute the voltage-controlled magnetism of the heterojunction to charge-dependent mechanism at the interface between ferroelectric and ferromagnetic layer. The study of voltage-controlled magnetic behaviors reveals the promising potential application of ferroelectric/ferromagnetic heterojunction in low-power and high-stability MRAM.

2. Experiment details

As shown in Fig. 1, the film stacks in this work are Si/TiN(10 nm)/$Hf_{0.5}Zr_{0.5}O_2$(10 nm)/Pt(0.5 nm)/Co(1 nm)/Ru(4 nm). The bottom electrode TiN is grown on 8-inch (1 inch = 2.54 cm) Si substrate by magnetron sputtering, then the $Hf_{0.5}Zr_{0.5}O_2$ (HZO) layer is deposited through atomic layer deposition (ALD) using deionized water, $Hf(NCH_3C_2H_5)_4$ and $Zr(NCH_3CH_5)_4$ as precursor, and the Pt, Co, Ru are grown by magnetron sputtering in sequence. After the film deposition, a 30-s annealing of temperature 400 °C under N_2 is performed by rapid thermal annealing (RTA) system. Then, a 50-nm Si_3N_4 is covered on the films as hard mask through plasma enhanced chemical vapor deposition (PECVD). Finally, the film stacks are processed by deep ultraviolet lithography (DUV), inductively coupled plasma (ICP) etching, passivation, interconnection and fabricated into Hall-bar device with the size of several hundred nanometers covered by passivation layer of Si_3N_4.

The basic magnetic property of films is performed on vibrating sample magnetometer (VSM), and the other measurement including anomalous Hall effect (AHE) test, voltage-controlled magnetism and ferroelectric property are performed on the Hall-bar device fabricated by 8-inch process.

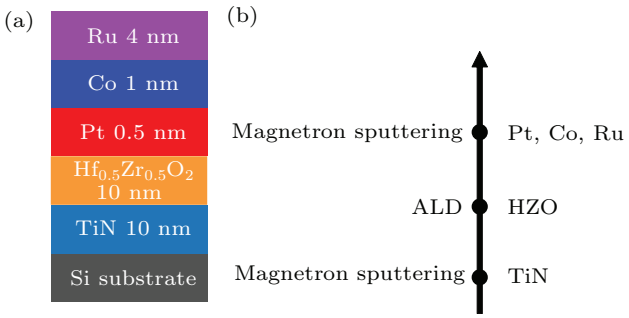


Fig. 1. (a) The film stacks and (b) the main processes of the film deposition.

3. Results and discussion

After the etching of hard mask, the whole morphology of Hall-bar structure is shown in Fig. 2(a) obtained by scanning electron microscope (SEM). As presented in Fig. 2(b), the width of channel is about 593 nm, the total area of the Hall-bar structure is about 100 μm^2. In order to get more details and prove the process, transmission electron microscopy (TEM) and related analysis are performed on the finished Hall-bar device. Figure 2(c) presents the cross-sectional TEM image of the film stacks, all the layers can be seen clearly and the HZO layer shows polycrystalline morphology which is a typical feature of HfO_2-based ferroelectric material.[14,15] Figure 2(d) exhibits the sidewall of Hall-bar structure from which we determine that the etching endpoint is in the HZO layer, which meets our expectation. The energy dispersive x-ray spectroscopy (EDX) is used to analyze distribution of elements, the slight indentations of Zr and Hf demonstrate the etching endpoint again. Obvious element diffusion is not found in the mapping results. Besides, we discover the appearance of some elements such as Hf, Zr, Pt, Ru at the sidewall which is caused by redeposition during etching.[16–19]

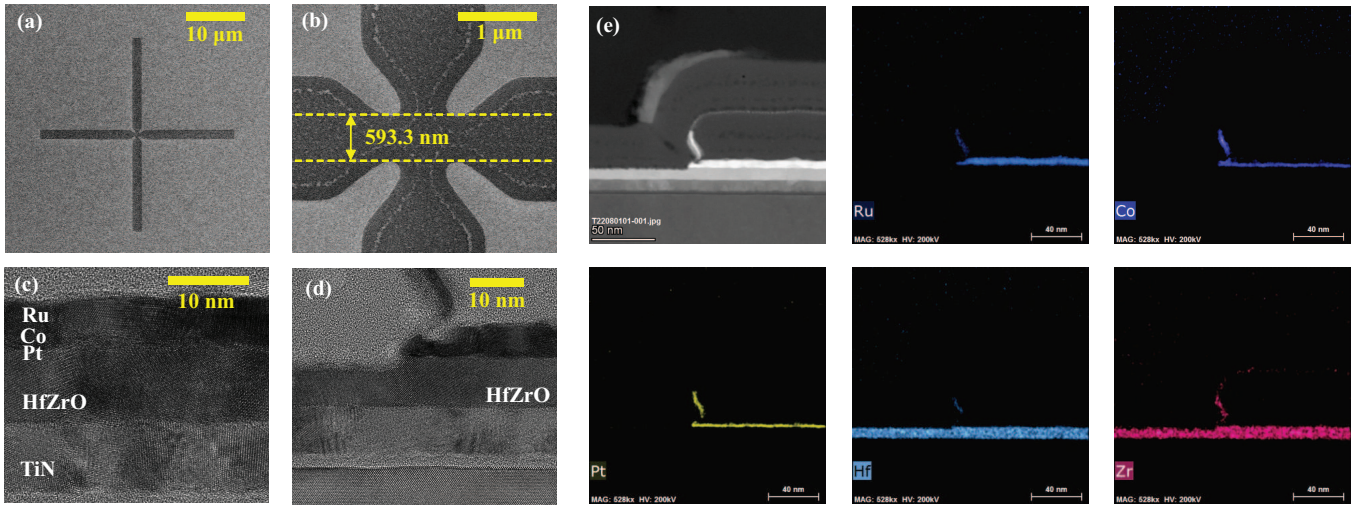


Fig. 2. (a) The top view of Hall-bar device obtained by SEM. (b) The channel SEM image of Hall-bar device. (c) The cross-sectional TEM image of film stacks. (d) The sidewall TEM image of Hall-bar device. (e) The distribution map of elements around sidewall.

The magnetic hysteresis loops of film stacks after RTA implemented by VSM are shown in Fig. 3. The magnetization reaches saturation at a smaller magnetic field and presents nearly 100% remanent magnetization under perpendicular magnetic field, while a larger saturation field and almost zero remanent magnetization are exhibited in the *M*–*H* curve measured under parallel magnetic field. The results indicate the film possesses PMA which mainly originates from the interfacial anisotropy.[20–22] From the measurement, we can get the saturation magnetization with the amplitude of 650 emu/cm^3.

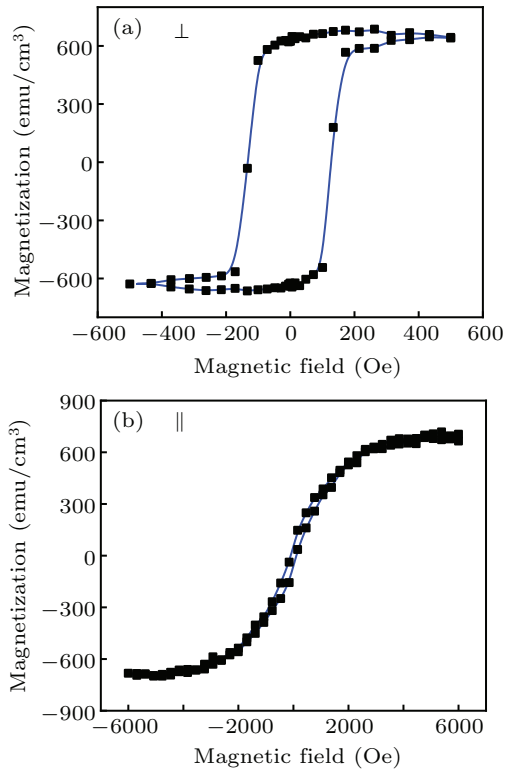


Fig. 3. The magnetic hysteresis loops of the film under perpendicular magnetic field (a) and parallel magnetic field (b). The unit 1 Oe = 79.5775 A·m^{-1}.

For the Hall-bar device fabricated by 8-inch process, AHE test is used to detect the kinetic magnetism. During the measurement, the Hall resistance along *y* axis is measured by Keithley 2450 while a 50-μA current generated by Keithley 2602B is applied on the *x* axis under perpendicular magnetic field as shown in Fig. 4(a). The AHE is an electrical transport measurement method which can be expressed as[23–25]

$$R_{\mathrm{H}} = \frac{R_0 B}{t} + \frac{4\pi R_{\mathrm{s}} M}{t}, \tag{1}$$

the anomalous Hall resistance R_{H} is comprised by ordinary part $(R_0 B/t)$ and anomalous part $(4\pi R_{\mathrm{s}} M/t)$, in which t is the thickness of current channel and B is external magnetic field. Usually, the anomalous Hall coefficient R_{s} is much larger than ordinary Hall coefficient R_0, as a result, the R_{H} is directly proportional to the perpendicular component of magnetization (M) which is used to study magnetic property. Like the test of VSM, the result in Fig. 4(b) also presents rectangular loop which indicates the PMA keeps stable as the scaling down of the film stacks, proving the reliability of process.

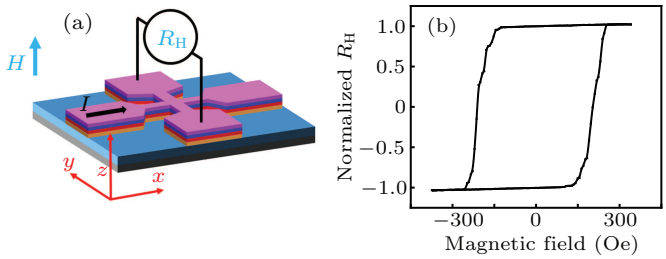


Fig. 4. (a) The diagram of AHE test. (b) The *R*–*H* curve of Hall-bar device under perpendicular field.

In order to investigate the effect on magnetic property caused by voltage, the AHE measurement with different voltage pulses are carried out. As shown in Fig. 5(a), the 9-ms voltage pulse supplied by Keithley 2602B is applied on the HZO layer through the top and bottom electrode, after cutting off the voltage pulse, an AHE measurement is performed. Before and after the voltage pulse, the resistance of HZO layer is measured to ensure its intact. The electric field that points from top to bottom electrode is defined as positive and *vice versa*. An obvious deformation of the AHE curve is observed under different voltage pulses. After a −3-V pulse, the curve around coercivity becomes more sloping, which has a smaller nucleation field ($H_{\mathrm{n}} \sim 15$ Oe) and coercivity ($H_{\mathrm{c}} \sim 160$ Oe), while the saturation field is almost unchanged ($H_{\mathrm{s}} \sim 254$ Oe). On the contrary, when a 3-V pulse is applied on the device, the curve becomes more sharper, which has a larger nucleation field ($H_{\mathrm{n}} \sim 172$ Oe) and coercivity ($H_{\mathrm{c}} \sim 225$ Oe), the saturation field still keeps stable. Besides, a slight decrease and increase in saturation Hall resistance under negative and positive voltage pulse also emerges. Figure 5(c) presents involved fields under different voltage pulses, the different slopes of three curves indicate the different responses to voltage pulse-the sensitive H_{N}, slightly changed H_{c} and stable H_{s}. The various discrete extent of the three fields shows the different switching processes under different voltage pulses.

The energy barrier E_{b} of magnetic layer can be expressed as the product of effective anisotropy energy density K_{u} and volume V.[26,27] We can get K_{u} by the difference in magnetization work between the direction of hard-axis and easy-axis written as follows (for PMA):[28,29]

$$K_{\mathrm{u}} = \mu_0 \left(\int_0^{M_{\mathrm{s}}} H_{\mathrm{in}} \, \mathrm{d}M_x - \int_0^{M_{\mathrm{s}}} H_{\mathrm{p}} \, \mathrm{d}M_z \right), \tag{2}$$

where the μ_0 is permeability of vacuum, M_{s} is saturation magnetization, H_{in} and H_{p} are in-plane and perpendicular magnetic fields, respectively. In this work, we can extract K_{u} from AHE measurement based on the following relation[30,31]

$$M_{\mathrm{s}}^2 = M_x^2 + M_z^2, \tag{3}$$

$$R_{\rm Nor} = \frac{R_{\rm H}}{R_{\rm max}} = \frac{M_z}{M_{\rm s}}, \tag{4}$$

$$K_{\rm u} = \mu_0 M_{\rm s}\left(\int_0^1 H_{\rm in}\,{\rm d}\sqrt{1-(R_{\rm Nor})^2} - \int_0^1 H_{\rm p}\,{\rm d}R_{\rm Nor}\right), \tag{5}$$

in which M_x and M_z are in-plane and perpendicular components of magnetization, $R_{\rm Nor}$ is the normalized Hall resistance. Figure 5(d) is the in-plane normalized R–H curves under different voltage pulses. Through the above method, the $K_{\rm u}$ under different voltage pulses is obtained and shown in Fig. 5(e). From the results, the voltage pulse has remarkable influence on the $K_{\rm u}$. The $K_{\rm u}$ is about 5.2×10^4 erg/cm^3 (1 erg = 10^{-7} J) after a −3-V pulse, which is reduced by 83% compared with initial value (3.2×10^5 erg/cm^3), and it is enhanced to 4.1×10^5 erg/cm^3 after a 3-V pulse, which is increased by 28%. The controlled coefficient calculated from fitting result is about 5.89×10^{-2} erg/(V·cm^2). The voltage-dependent $K_{\rm u}$ implies bidirectional change in energy barrier based on the polarity of voltage. As depicted above, there is no voltage on the HZO layer during AHE test, therefore, the effect on magnetic property and energy barrier is non-volatile. In general, a reversible, non-volatile modulation on magnetic property, and energy barrier by voltage pulse can be realized in the HZO/Co heterojunction.

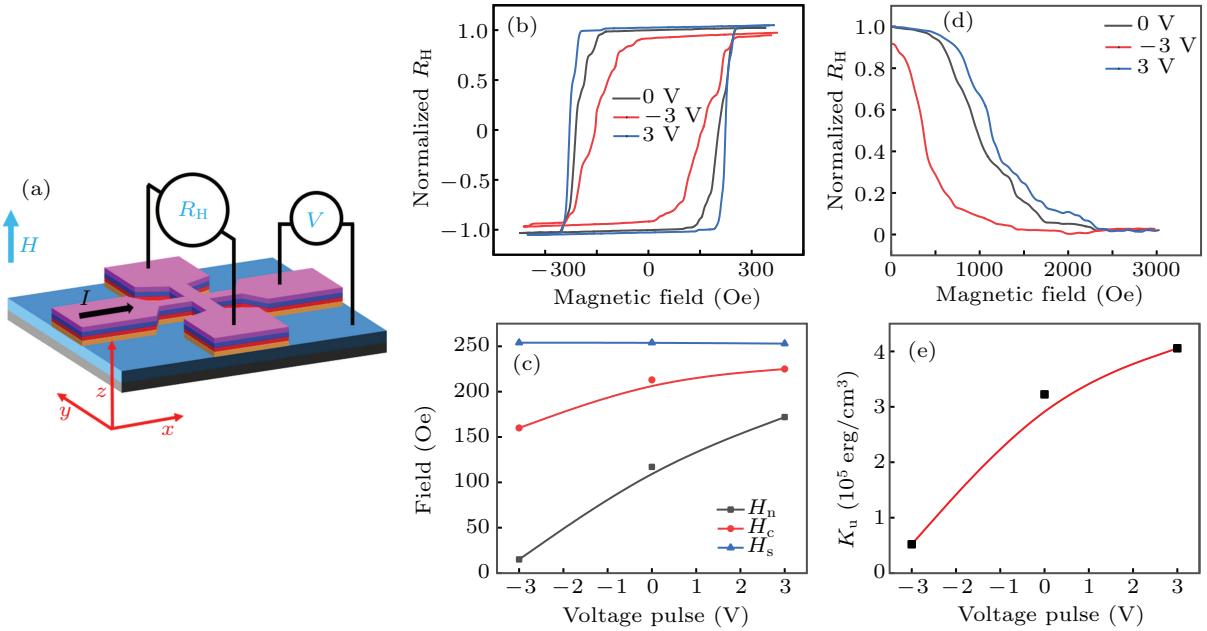


Fig. 5. (a) The test diagram of voltage-controlled magnetism. (b) The R–H curves under perpendicular field with different voltage pulses. (c) The nucleation field, coercivity and saturation field under different voltage pulses. (d) The R–H curves under in-plane field with different voltage pulses. (e) Voltage-dependent effective anisotropy energy density.

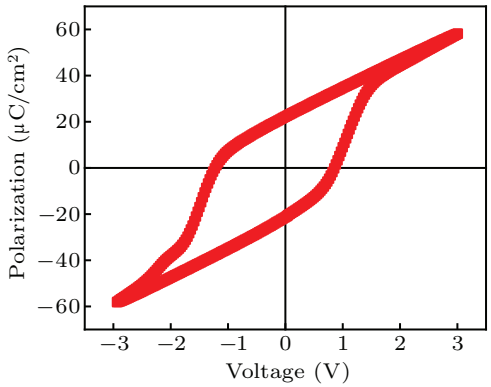


Fig. 6. The P–V curve of Hall-bar device with the amplitude of 3 V.

To explore the mechanism of voltage-dependent magnetism, the ferroelectric property is measured on Hall-bar device by ferroelectric tester (TF Analyzer 3000). A 1-kHz triangle wave signal with the amplitude of 3 V is applied on the device through the top and bottom electrode. The voltage-dependent polarization is shown in Fig. 6, hysteresis loop of P–V curve is a characteristic of ferroelectric property, indicating the reasonable design of film stacks and process. The remanent polarization is about 21 μC/cm^2 which demonstrates the Hall-bar device possesses good ferroelectric property.

The charge-mediated modulation is a common mechanism which often refers to charge, spin and orbital degrees of freedom at the interface. In ferroelectric/ferromagnetic heterojunction, the change in interfacial electron density at ferromagnetic layer caused by ferroelectric polarization will induce the shift of Fermi level, leading to the change in the state distribution of spin electron, thus modulating magnetic property.[32,33] Duan *et al.* pointed that the atoms displacement involved in the reversal of ferroelectric polarization changes the chemical bonding at the interface, which has a significant effect on magnetism.[34,35] For some magnetic material systems, the surface magnetic anisotropy is sensitive to variation in interfacial electron density because of the spin–orbit coupling caused by interfacial orbital reconstruction.[36,37]

As depicted in Fig. 7, when a voltage pulse is applied on the Hall-bar device, the HZO ferroelectric layer is polarized and some bound charges are formed at the interface. Because of the Coulomb force, the electrons at metal layer will be attracted or repelled, thus inducing accumulation or dissipation of electrons at the interface. The variation in electron concentration is restricted to several angstroms due to charge screening in metal. In film deposition, a 0.5-nm Pt layer is inserted between HZO and Co layer to construct a Co/Pt interface which can provide interfacial anisotropy and promote PMA. The Pt spacer may weaken the effect on Co layer caused by the change in electron concentration from the view of conventional charge-mediated mechanisms. While Jia *et al.* proposed a novel mechanism of interfacial spiral spin density in ferroelectric/ferromagnetic heterojunction, which can affect magnetism with a thickness about tens of nanometers through spin diffusion.[38] Subsequently, the mechanism has been demonstrated experimentally.[39] These results provide a new foundation for works about charge-mediated mechanism in ferroelectric/ferromagnetic heterojunction. In this work, we think a local spiral spin density related to interfacial charges is formed and a spin rearrangement is induced within a larger length which reaches the Co layer through spin diffusion. Therefore, the voltage-controlled magnetism is realized by the change in interfacial electron density across the Pt spacer.

As shown in Fig. 5(c), the H_n, H_c, and H_s present different responds to voltage pulses, which may be related to different interactions between magnetic domains and ferroelectric domains. During the process of magnetization, some magnetic domains around the edge switch under larger external magnetic field, which decides the value of H_s. And the ferroelectricity degradation may happen in some ferroelectric domains around the edge of HZO layer caused by etching damage.[40] Therefore, these magnetic domains around the edge are not affected by ferroelectricity and present stable H_s. Another possibility is that the defects at the interface have pinning effect on adjacent magnetic domains and ferroelectric domains simultaneously, these pinned magnetic domains need larger external magnetic field (H_s) to switch and the pinned ferroelectric domains are hard to switch during polarization. Thus, there are almost no couplings between these magnetic and ferroelectric domains. The magnetization switching behaviors of other magnetic domains are controlled by ferroelectricity and show voltage-dependent H_n and H_c as a result of statistics.

Because the non-volatile characteristic is one of ferroelectric properties, a reversible and non-volatile modulation in magnetic property can be realized in HZO/Co multiferroic heterojunction. Moreover, the voltage-related K_u is proved above, which means energy barrier is controllable as shown in Fig. 7. In MRAM, the lower energy barrier is desired during data writing while a higher energy barrier favors data retention.

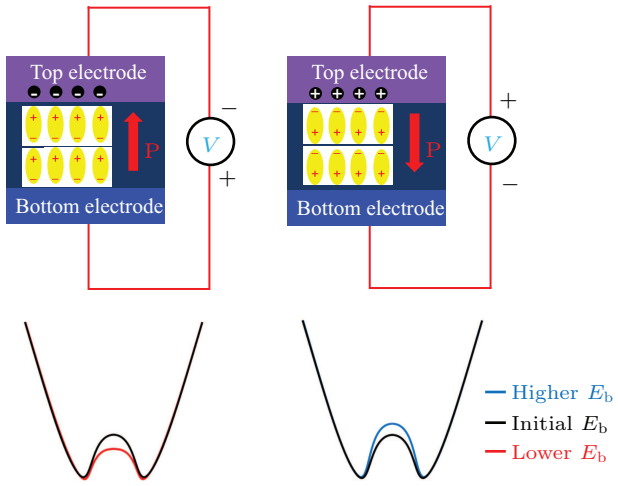


Fig. 7. The interfacial charges under different voltage pulses and corresponding energy barrier.

4. Conclusion

We investigated the voltage-controlled magnetism in Hall-bar device with the size of several hundred nanometers constructed by HZO/Co multiferroic heterojunction systematically in this work. The nucleation field, coercivity, and saturation field of *R*–*H* curve under perpendicular field show different responses to voltage pulse, which is considered to different interactions between magnetic domains and ferroelectric domains. Through ferroelectric test and analysis, we attribute the voltage-dependent magnetism to interfacial charge caused by ferroelectric polarization. Besides, we calculated the effective anisotropy energy density under different voltage pulses. Compared with the initial value, a decrease of 83% under −3 V and increase of 28% under 3 V are observed. All the above variations are non-volatile because of the non-volatile characteristic of ferroelectric property. The controllable effective anisotropy energy density means energy barrier can be modulated by voltage pulse. For MRAM, a lower energy barrier denotes lower power consumption during data writing while a higher energy barrier indicates better stability which is beneficial to data retention. The research in this work shows an effective method to control energy barrier, proposing a scenario for low-power and high-stability MRAM.

Acknowledgements

Project supported by Strategic Priority Research Program of the Chinese Academy of Sciences (Grant No. XDA18000000), the Fund from the Youth Innovation Promotion Association of the Chinese Academy of Sciences (Grant No. 2015097), and Guangzhou City Research and Development Program in Key Fields (Grant No. 202103020001).

References

[1] He H, Zhao J T, Luo Z L, Yang Y J, Xu H, Hong B, Wang L X, Wang R X and Gao C 2016 *Chin. Phys. Lett.* **33** 67502

[2] Huang Q, Dong Y, Zhao X, Wang J, Chen Y, Bai L, Dai Y, Dai Y, Yan S and Tian Y 2020 *Adv. Electron. Mater.* **6** 2070013

[3] Li Y, Luo W, Zhu L, Zhao J and Wang K 2015 *J. Magn. Magn. Mater.* **375** 148

[4] Ren J, Li J, Zhang S, Li J, Su W, Wang D, Cao Q and Du Y 2022 *Chin. Phys. B* **31** 077502

[5] Nozaki T, Yamamoto T, Tamaru S, Kubota H, Fukushima A, Suzuki Y and Yuasa S 2018 *APL Mater.* **6** 026101

[6] Shiota Y, Bonell F, Miwa S, Mizuochi N, Shinjo T and Suzuki Y 2013 *Appl. Phys. Lett.* **103** 082410

[7] Song J, Ahmed I, Zhao Z, Zhang D, Sapatnekar S S, Wang J P and Kim C H 2018 *IEEE Journal on Exploratory Solid-State Computational Devices and Circuits* **4** 76

[8] Bauer U, Yao L, Tan A J, Agrawal P, Emori S, Tuller H L, van Dijken S and Beach G S 2015 *Nat. Mater.* **14** 174

[9] Gilbert D A, Grutter A J, Arenholz E, Liu K, Kirby B J, Borchers J A and Maranville B B 2016 *Nat. Commun.* **7** 12264

[10] Quintana A, Menendez E, Liedke M O, Butterling M, Wagner A, Sireus V, Torruella P, Estrade S, Peiro F, Dendooven J, Detavernier C, Murray P D, Gilbert D A, Liu K, Pellicer E, Nogues J and Sort J 2018 *ACS Nano* **12** 10291

[11] Rojas J, Quintana A, Lopeandía A, Salguero J, Costa-Krämer J L, Abad L, Liedke M O, Butterling M, Wagner A, Henderick L, Dendooven J, Detavernier C, Sort J and Menéndez E 2020 *Adv. Funct. Mater.* **30** 2003704

[12] Daumont C, Wolfman J, Autret-Lambert C, Andreazza P and Negulescu B 2018 *Appl. Phys. Lett.* **112** 112401

[13] Vermeulen B F, Ciubotaru F, Popovici M I, Swerts J, Couet S, Radu I P, Stancu A, Temst K, Groeseneken G, Adelmann C and Martens K M 2019 *ACS Appl. Mater. Interfaces* **11** 34385

[14] Muller J, Boscke T S, Schroder U, Mueller S, Brauhaus D, Bottger U, Frey L and Mikolajick T 2012 *Nano Lett.* **12** 4318

[15] Tian G, Xu G, Yin H, Yan G, Zhang Z, Li L, Sun X, Chen J, Zhang Y and Bi J 2022 *Adv. Mater. Interfaces* **9** 2102351

[16] Desbiolles B X E, Bertsch A and Renaud P 2019 *Microsyst. Nanoeng.* **5** 11

[17] Islam R, Cui B and Miao G X 2020 *J. Vac. Sci. Technol. B* **38** 050801

[18] Kinoshita K, Utsumi H, Suemitsu K, Hada H and Sugibayashi T 2010 *Jpn. J. Appl. Phys.* **49** 08JB02

[19] Park S, Yang K, Lee H, Kim D, Baek J, Shim T, Park J and Yeom G 2017 *ECS J. Solid State Sci. Technol.* **6** N148

[20] Lau Y C, Chi Z, Taniguchi T, Kawaguchi M, Shibata G, Kawamura N, Suzuki M, Fukami S, Fujimori A, Ohno H and Hayashi M 2019 *Phys. Rev. Mater.* **3** 104419

[21] Nistor L E, Rodmacq B, Auffret S and Dieny B 2009 *Appl. Phys. Lett.* **94** 012512

[22] Sun Y, Ba Y, Chen A, He W, Wang W, Zheng X, Zou L, Zhang Y, Yang Q, Yan L, Feng C, Zhang Q, Cai J, Wu W, Liu M, Gu L, Cheng Z, Nan C W, Qiu Z, Wu Y, Li J and Zhao Y 2017 *ACS Appl. Mater. Interfaces* **9** 10855

[23] Moon K W, Lee J C, Choe S B and Shin K H 2009 *Rev. Sci. Instrum.* **80** 113904

[24] Shepley P M, Rushforth A W, Wang M, Burnell G and Moore T A 2015 *Sci. Rep.* **5** 7921

[25] Zhu T 2014 *Chin. Phys. B* **23** 047504

[26] Liu H F, Ali S S and Han X F 2014 *Chin. Phys. B* **23** 077501

[27] Wu X W, Guslienko K Y, Chantrell R W and Weller D 2003 *Appl. Phys. Lett.* **82** 3475

[28] Shiota Y, Murakami S, Bonell F, Nozaki T, Shinjo T and Suzuki Y 2011 *Appl. Phys. Express* **4** 043005

[29] Zhu J, Katine J A, Rowlands G E, Chen Y J, Duan Z, Alzate J G, Upadhyaya P, Langer J, Amiri P K, Wang K L and Krivorotov I N 2012 *Phys. Rev. Lett.* **108** 197203

[30] Li X, Fitzell K, Wu D, Karaba C T, Buditama A, Yu G, Wong K L, Altieri N, Grezes C, Kioussis N, Tolbert S, Zhang Z, Chang J P, Khalili Amiri P and Wang K L 2017 *Appl. Phys. Lett.* **110** 052401

[31] Wang L, Li X, Sasaki T, Wong K, Yu G, Peng S, Zhao C, Ohkubo T, Hono K, Zhao W and Wang K 2020 *Sci. Chin.-Phys. Mech. Astron.* **63** 277512

[32] Vaz C A 2012 *J. Phys.: Condens. Matter* **24** 333201

[33] Velev J P, Jaswal S S and Tsymbal E Y 2011 *Philos. Trans. A: Math. Phys. Eng. Sci.* **369** 3069

[34] Duan C G, Jaswal S S and Tsymbal E Y 2006 *Phys. Rev. Lett.* **97** 047201

[35] Duan C G, Velev J P, Sabirianov R F, Zhu Z, Chu J, Jaswal S S and Tsymbal E Y 2008 *Phys. Rev. Lett.* **101** 137201

[36] Haraguchi S, Tsujikawa M, Gotou J and Oda T 2011 *J. Phys. D: Appl. Phys.* **44** 064005

[37] Nakamura K, Shimabukuro R, Fujiwara Y, Akiyama T, Ito T and Freeman A J 2009 *Phys. Rev. Lett.* **102** 187201

[38] Jia C L, Wei T L, Jiang C J, Xue D S, Sukhov A and Berakdar J 2014 *Phys. Rev. B* **90** 054423

[39] Zhou C, Shen L, Liu M, Gao C, Jia C, Jiang C and Xue D 2018 *Adv. Funct. Mater.* **28** 1707027

[40] Lin Y D, Yeh P C, Tang Y T, Su J W, Yang H Y, Chen Y H, Lin C P, Yeh P S, Chen J C and Tzeng P J 2021 *IEEE International Electron Devices Meeting (IEDM)*, December 13–15, 2021, San Francisco, USA, p. 6.4.1